Quantifying the impact of network structure on speed and accuracy in collective decision-making

Bryan C. Daniels[1] and Pawel Romanczuk[2,3]

[1]ASU–SFI Center for Biosocial Complex Systems, Arizona State University, Tempe, Arizona, USA
[2]Institute for Theoretical Biology, Department of Biology, Humboldt Universität zu Berlin, Germany
[3]Bernstein Center for Computational Neuroscience, Berlin, Germany

Found in varied contexts from neurons to ants to fish, binary decision-making is one of the simplest forms of collective computation. In this process, information collected by individuals about an uncertain environment is accumulated to guide behavior at the aggregate scale. We study binary decision-making dynamics in networks responding to inputs with small signal-to-noise ratios, looking for quantitative measures of collectivity that control decision-making performance. We find that decision accuracy is controlled largely by three factors: the leading eigenvalue of the network adjacency matrix, the corresponding eigenvector's participation ratio, and distance from the corresponding symmetry-breaking bifurcation. This allows us to predict how decision-making performance scales in large networks based on their spectral properties. Specifically, we explore the effects of localization caused by the hierarchical assortative structure of a "rich club" topology. This gives insight into the tradeoffs involved in the higher-order structure found in living networks performing collective computations.

Keywords: collective computation, neural networks, symmetry breaking transition, stochastic dynamical systems, rich club

Introduction

Collective intelligence refers to the ability of groups of individual components to process environmental information and successfully perform adaptive functions at a larger collective scale. Building a coherent framework for understanding distributed functionality is challenging in that the internal structure of natural and engineered collectives varies strongly, from quasi-homogeneous systems like swarms of identical robots, to fish-schools consisting of similarly behaving individuals but with persistent behavioral differences ("personalities") [1,2] or different prior information [3,4], to strongly heterogeneous and hierarchical systems like primate societies [5,6] or neurons in a brain [7,8]. Facing this diversity, a key challenge for building a better abstract understanding of collective intelligence is to determine which details of such systems are most important to collective function and which are incidental and can be ignored. In this way,

we are searching for measures that usefully quantify "collectivity" across a broad continuum of complex systems.

In addition to diversity in heterogeneity and communication structure, myriad types of functions may be implemented in a collective system, ranging in complexity from simple majority consensus to high-level abstract information processing. Here we focus on a particularly simple function—making a correct binary decision about the sign of a noisy distributed input—and look for network statistics that delineate the full range of strategies that can be used to successfully perform this collective function.

Past experimental investigations of collective decision-making have mostly not addressed network structure, instead assuming all-to-all coupling and focusing on optimal rules for aggregating decisions made by individuals [9–13]. However, an increasing number of studies are beginning to investigate non-trivial network structures [14–17]. For example, Kearns et al [14] look at the effect of varying network structure in consensus formation in human groups. They find, e.g., that "preferential attachment" networks lead to faster consensus than Erdos–Renyi.

Theoretically, many examples of collective decision-making can be effectively described using networks of coupled dynamical components. Structural properties of such networks and how they affect self-organization and collective behavior have long been a focus of complex systems research (see e.g. [18–21]). Particularly well studied are effects of network structure on emergent dynamics in the context of synchronization and consensus formation [18, 19]. Theoretical research often aims to map the phase diagram of system dynamics as a function of underlying network structure parameters, for example to identify regions of synchronized versus random dynamics (see e.g. [19] and references therein). This language of phase diagrams, originating in statistical physics, has also been used to hypothesize that in order to ensure optimal information processing, collective systems should operate near phase transitions (critical manifolds) [22, 23]. [1]

Corresponding theoretical insights have driven the systematic analysis of structural properties of artificial and real-world networks, including node and degree heterogeneity [25] and structural hierarchies [26, 27]. In particular, many real-world collective systems exhibit a "rich club" (core-periphery) structure, with examples coming from neuroscience [7, 8, 28–30], social science, and biochemistry [12, 31]. The rich club refers to a subset of nodes that a) have a larger (in-)degree and b) are more likely to be connected to other rich club nodes than in an otherwise random wiring. It has been argued that such a core-periphery topology may play an important role for the function of complex information processing systems (see e.g. [7, 30, 32]).

The dynamical effects of network structure have been explored largely in the context of synchronization or consensus, the problem of collective agreement. Extending to the problem of decision-making also requires a notion of correctness: we want a system that not only produces collective agreement on any consensus state, but on the correct state, given a source of input information. Binary collective decision-making in this sense maps naturally onto "noisy integrator" models, such as leaky integration to bound (Ornstein–Ullenbeck [33]) and related models with stable attractors representing decision states [34, 35]. A general constraint for any such decision-making system is the tradeoff between speed and accuracy [33, 36, 37]. Recently, it has been shown that the speed–accuracy tradeoff in simple collective decision models can be quantified in terms of distance from a bifurcation [35, 38].

Motivated by the above findings, we focus in this work on the question of how a rich-club structure affects

---

[1]In some large N limits, hierarchical modular networks can have infinitely many localized modes corresponding to critical coupling strength values over a continuous range—this produces a so-called "Griffiths phase" [24]. We do not focus on this here because we anticipate our methods will be most useful applied to known finite networks.

the speed and accuracy of collective decision-making. In particular, we look for network statistics that capture the most important properties controlling collective performance in decision dynamics.

Results

Collective decision-making model

A simple minimal model of distributed decision-making defines dynamics for the internal noisy states of individual components, each of which receives the same input signal I, recovers to a null state on a timescale τ, and is affected by its neighbors through a saturating function of its neighbors' states [35, 38]:

$$\frac{ds_i}{dt} = -\frac{s_i}{\tau} + \frac{\mu}{\tau} \sum_j A_{ij} \tanh(s_j) + \frac{I}{\tau} + \xi, \tag{1}$$

where I is an input signal given uniformly to every node and ξ is uncorrelated Gaussian noise with $\langle \xi(t)\xi(t + \Delta t) \rangle = \sigma^2 \tau^{-1} \delta(\Delta t)$. We explicitly write the differential equations in terms of an overall timescale τ; in describing neural dynamics, for example, we expect τ to be on the order of tens of milliseconds.

We initialize the system in a state $\vec{s}_0$ that, in the case of zero noise, corresponds to a fixed point undergoing a pitchfork bifurcation as a function of the coupling strength μ. This bifurcation separates the case of a single stable fixed point at $\vec{s}_0$ and the case of two distinct stable fixed points at $\vec{s}_0 \pm \epsilon \hat{e}_c$, which we treat as decision states (where $\hat{e}_c$ is the unit vector pointing in the direction in which the decision states emerge from $\vec{s}_0$ at the bifurcation). We focus here on the simplest such bifurcation,[2] which occurs at $\vec{s}_0 = \vec{0}$.

To test how the existence of higher-order structure changes the decision-making performance, we vary the adjacency matrix A to test symmetric networks with fixed size N and total number of edges, changing only the degree distribution and higher-order structure (Figure 1). First, a "rich club" network is created through a random generation of a fixed number of edges from the $N(N-1)$ possible edges, where edges between N_{rich} core nodes are biased to be more likely to appear by a factor b_{rich}. A corresponding network that has exactly the same degree distribution but no rich club is then created by randomly swapping existing edges. Finally, we test an Erdos–Renyi variant in which all possible edges are equally likely. We use the same three specific example networks shown in Figure 1 in simulations throughout the paper; results are qualitatively similar for other networks sampled from each ensemble.

Speed–accuracy tradeoff

We test each network in its ability to integrate information about a signal that is small compared to the noise and then retain that information after the signal is removed. We define accuracy in terms of whether the system ends the simulation near the correct decision state, the one that lies in the direction of the input $+I$ (instead of $-I$). Specifically, we test whether the sign of the final state along the unstable dimension, $(\vec{s}_{\text{final}} - \vec{s}_0) \cdot \hat{e}_c$, is the same as the sign of the input along that dimension, $I\vec{1} \cdot \hat{e}_c$.

As in previous studies using a similar model [35, 38] (and across a wide variety of systems in general [36, 37, 39]), we expect to find a speed–accuracy tradeoff: Slow dynamics should produce better accuracy,

---

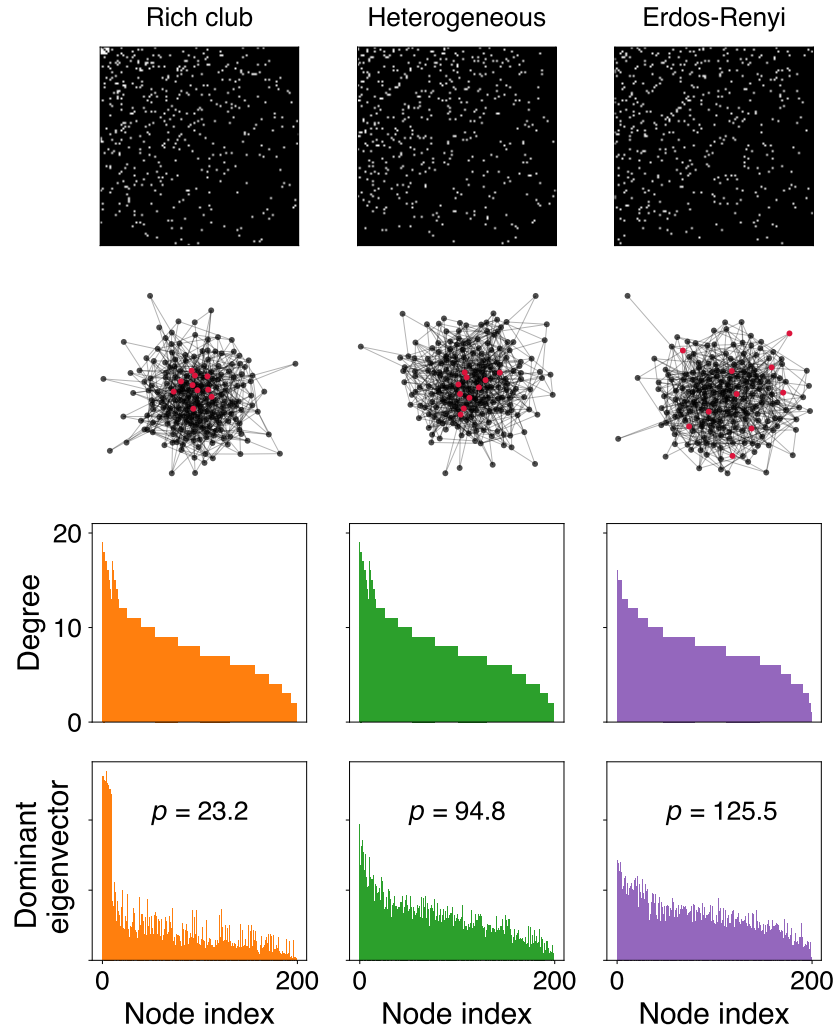[2] Tuning a second control parameter can locate more general pitchfork bifurcations; see [38].

Figure 1: **Three random networks with varying higher-order network structure.** All networks share the same size ($N = 200$) and total number of edges (800). The "rich club" network is generated such that a core group of 10 nodes have increased probability of edges within the group ($b_{\text{rich}} = 257$); the "heterogeneous" network has identical degree distribution to the rich club network but with edges otherwise randomized; and the "Erdos–Renyi" network is selected such that all possible edges have equal probability. We characterize each network using its adjacency matrix (top row), network diagram (second row), degree distribution (third row), and dominant eigenvector and corresponding participation ratio p (bottom row). Throughout the figure, nodes are ordered first by core and periphery groups and then sorted by degree. Core nodes are highlighted in red in the network diagrams.
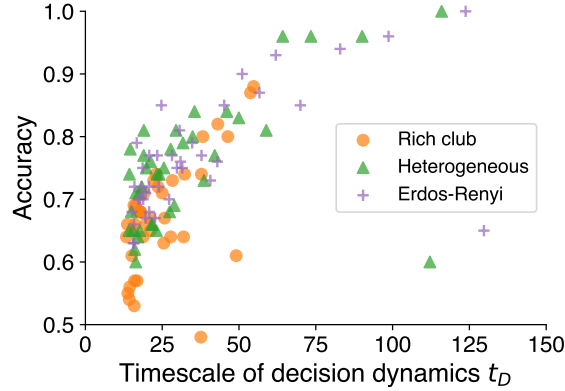
Figure 2: **Speed–accuracy tradeoff.** Simulations show that maximal accuracy of a noisy collective decision occurs when the decision process happens over a longer timescale, lengthening the time over which the system remains sensitive to the input. Here and in other plots unless otherwise specified, $\tau = 1$, $\sigma = 0.05$, $I = 0.001$, the duration of the signal $= 200\tau$, the total simulation time $= 2000\tau$, $\Delta\mu$ ranges from 0 to 0.04, and we average over 100 simulations for each network.

as the system is able to integrate the input over a longer time before fixating within a single decision state, whereas fast dynamics produce a decision based primarily on noise.

To quantify the speed of the decision, we measure a characteristic time t_D over which the system approaches the final decision fixed point. We first define the two decision states $\vec{s}^*_\pm$ as the stable fixed points of the dynamics in Eq. (1) with zero input and zero noise.[3] We then define the decision timescale t_D as the first time the state $\vec{s}$ reaches halfway to the decision state $\vec{s}^*$ along the dimension $\hat{s}^* = (\vec{s}^* - \vec{s}_0)/|\vec{s}^* - \vec{s}_0|$.

As expected, our simulations show a speed–accuracy tradeoff as we vary the overall connection strength μ, shown in Figure 2. When tuned to a given decision timescale, the accuracy is largely unaffected by network structure. The highest accuracy is observed when the system supports long timescale dynamics.

Given that performance is largely controlled by the decision timescale t_D, we would like to understand how the network structure, defined by the adjacency matrix A, controls t_D. We expect that the largest timescales will occur near the symmetry-breaking transition that creates the two decision states.

Locating the transition and decision states

First, we must locate the relevant pitchfork bifurcation, which controls the transition between dynamics in which node states are not correlated over long times (when μ is small and interactions between nodes are weak) into dynamics in which a nodes can collectively store a long-term memory (when μ is large enough that interactions support a self-reinforcing consensus state). With zero input and zero noise, it is straightforward to find this transition, by analyzing how a small perturbation $\delta\vec{s}$ to the initial state $\vec{s}_0$

---

[3] In the case here with $\vec{s}_0 = \vec{0}$, the two decision states are related simply by an inversion symmetry: $\vec{s}^*_+ = -\vec{s}^*_-$. Sufficiently close to the bifurcation, we expect analogous results for the speed–accuracy tradeoff even in more complicated cases where this symmetry does not hold [38].
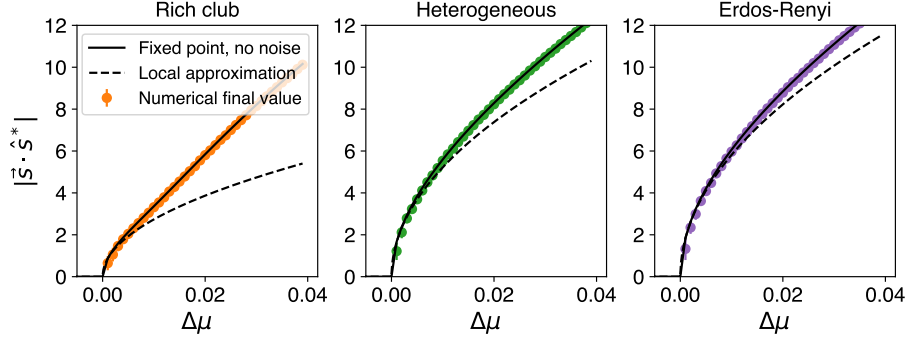
Figure 3: **A local approximation for the location of decision state fixed points.** Analytical approximations are compared to the simulated norm of the steady-state vector versus coupling strength. A local approximation using only the eigenvalue λ_c and participation ratio p [Eq. (5)] is shown as a dashed line. The numerical solution of the zero input, zero noise case [Eq. (1) with $I = \sigma^2 = 0$] is shown as a solid line. The average final state in simulations, including noise but no input, is shown as colored points, with errorbars (not visible for most points) corresponding to standard deviation of the mean.

changes under the dynamics:

$$\tau \frac{d\delta\vec{s}}{dt} = -\delta\vec{s} + \mu A \delta\vec{s} = (\mu A - \mathcal{I})\delta\vec{s}, \tag{2}$$

where $\mathcal{I}$ is the identity matrix. Then the behavior is most easily analyzed in the basis of eigenvectors of A: the dynamics along eigenvector $\hat{e}_\lambda$ are given by

$$\tau \frac{d\delta\hat{e}_\lambda}{dt} = (\mu\lambda - 1)\delta\hat{e}_\lambda. \tag{3}$$

Thus the initial state $\vec{s}_0$ will be stable until μ becomes large enough to make $(\mu\lambda - 1)$ positive. In other words, as we expect from basic linear stability analysis [40], the critical value of μ at which $\vec{s}_0$ first becomes unstable is controlled by the largest eigenvalue λ_c of A:

$$\mu_c = \lambda_c^{-1}. \tag{4}$$

The symmetry between positive and negative values of s means that this is a pitchfork bifurcation, and two stable fixed points emerge from the unstable fixed point along the dimension of the eigenvector corresponding to λ_c.

The distance between each stable fixed point (decision state) and the unstable starting point $\vec{s}_0$ grows as a function of μ: Near the transition [see Appendix Eq. (8)],

$$||\vec{s}^* - \vec{s}_0|| \approx \sqrt{3\Delta\mu\lambda_c p} = \sqrt{3\bar{\mu}p}, \tag{5}$$

where $\Delta\mu = \mu - \mu_c$, $\bar{\mu} = \Delta\mu/\mu_c$ is the reduced distance from the transition, and $p = 1/|(\hat{e}_c)^4|$ characterizes the distributedness of the eigenvector $\hat{e}_c$ corresponding to the leading eigenvalue λ_c.

The value p sets the scale of the distance between the collective decision states, and it corresponds roughly to the number of individual nodes contributing to the mode (see the bottom row of Figure 1). In general,
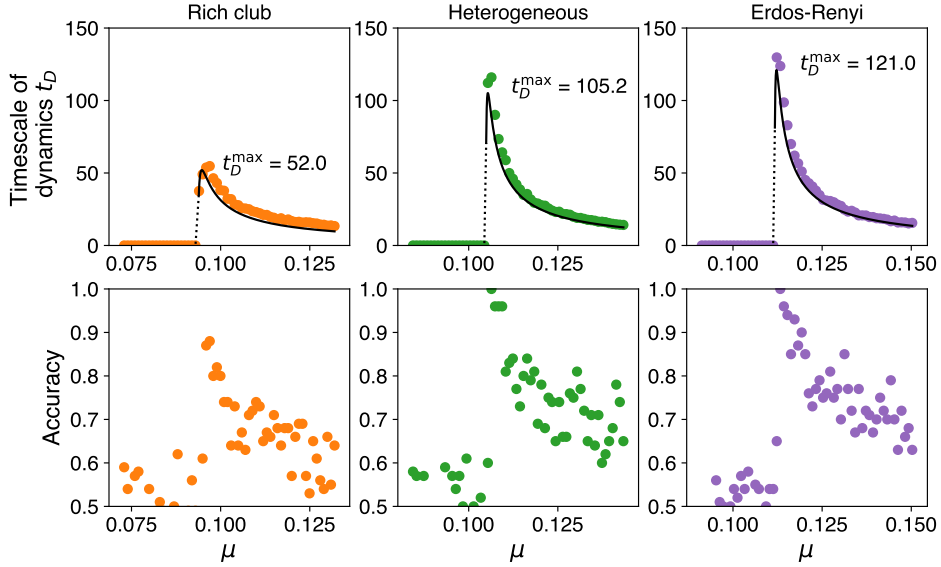
Figure 4: **Predicting the timescale of the decision.** Critical slowing down increases the timescale of motion toward the decision state (top row) when the coupling strength μ is tuned near the symmetry-breaking bifurcation. Simulation results are shown as colored points, and an analytical approximation of t_D [Eq. (13)] is shown as dashed and solid black lines. The approximate maximum timescale $t_D^{\max}$, expected to set an upper limit on accuracy, is proportional to $\sqrt{p}$. Accuracy also peaks near the transition (bottom row).

p varies between 1 for a completely localized mode and N for a completely delocalized mode (produced, for example, by homogeneous all-to-all coupling). The inverse of p appears in studies of localization in random matrix theory, where it has been called the "inverse participation ratio" [41, 42]; we therefore call p the participation ratio.

Figure 3 compares this zero-noise local approximation to the zero-noise numerical solution for the fixed point $\vec{s}^*$ and to the final state of the simulation including noise.[4] For each network, the transition occurs at the expected μ_c and with the expected local dependence on $\Delta\mu$. Because the largest timescales also occur near the transition, this local analysis will allow us to approximate the maximal decision timescale in the next section.[5]

Predicting the timescale of the decision

In the absence of noise, the timescale of the decision is expected to diverge at the transition, because the fixed point at the origin becomes marginally stable. With noise, this is smoothed out in a predictable way,

---

[4] Noise also affects the location of the transition. In our simulations here we use a small noise parameter σ (with input signal I even smaller to achieve a small signal-to-noise ratio); this means the effect of noise on the transition location is minimal on the scales we test. We calculate the lowest-order correction to μ_c in the Appendix and find that it is on the order of 10^{-3} for the plotted cases.

[5] Note that, in the rich club network, increasing the coupling beyond the scale shown in Figure 3 can also create bistability in the peripheral nodes. These cases have four stable fixed points, two of which correspond to the core and periphery nodes coming to consensus on conflicting decisions, and two in which core and periphery disagree. In our current setup, these cases do not change our analysis because the core always decides first, biasing the remainder of the system.

leading to a simple equation for the timescale derived in the Appendix, Eq. (13). Roughly, the timescale is determined by a combination of the distance between the two decision states (proportional to $\sqrt{\Delta\mu}$), the characteristic timescale of exponential growth away from the unstable fixed point (proportional to $\Delta\mu^{-1}$), and the characteristic speed of motion due solely to noise (proportional to σ).

In Figure 4, we demonstrate that the decision timescale is well-approximated by Eq. (13). As we saw before in Figure 2, longer timescales correspond to better accuracy. Further, this analysis allows us to predict the maximal decision timescale supported by a given network under a given level of noise σ; we find [see Appendix Eq. (14)]

$$t_D^{\max} \propto \sqrt{p}/\sigma; \tag{6}$$

that is, the timescale supported by the collective mode scales with the square root of the participation ratio. Consequently, due to the fundamental speed–accuracy tradeoff, p becomes a useful quantification of higher order network structure that sets a limit on collective decision accuracy.

Discussion

We study here a collective decision process that relies on the phenomenon of critical slowing down, a mechanism for creating long-timescale dynamics. In the case of small signal-to-noise ratio, decision accuracy is limited by the timescale of collective dynamics, and the system must be tuned near a symmetry-breaking bifurcation to successfully integrate information into an accurate decision. Varying the distance from the bifurcation $\Delta\mu$ traces out a speed–accuracy tradeoff (Figure 2).

In the spirit of quantifying collectivity, our aim is to characterize the aspects of network connectivity that control this timescale and therefore place limits on collective decision accuracy. We find that the most important factors characterize the normal mode of the network that is least stable. This is the mode that first becomes unstable as interaction strengths are increased, thereby leading to bistability that encodes a binary decision. First, the leading eigenvalue λ_c, effectively a measure of the connectivity of individuals participating in the mode, sets the scale of the critical coupling μ_c required for reinforcing the decision state. Second, the participation ratio p of the corresponding eigenvector is a measure of the number of individuals participating in the mode.

Our main result is to identify λ_c and p as important measures for quantifying collective behavior in heterogeneous networks. Given any detailed network structure, these two simple statistics encapsulate the network's ability to create long-timescale dynamics. This allows us to predict how collective timescales behave across a variety of network structures. For instance, the maximal decision timescale that can be produced by the critical slowing mechanism increases in a predictable way as more individual nodes are allowed to participate in the unstable mode, scaling as $\sqrt{p}$. This fits with our rough intuition, as we expect that the effects of noise will shrink in a group of N individuals as $1/\sqrt{N}$.

Generally, our results resonate with recent studies that focus on low-dimensional collective modes controlling the most important aspects of distributed computation in biological networks [43,44]. The importance of the principal eigenvalue and corresponding (inverse) participation ratio hints at connections between our model of decision-making and related characterizations of disease spreading [45], correlations in financial data [41], and Anderson localization in condensed matter physics [46].

Our motivation began with understanding the functional consequences of rich-club structure and criticality in the brain. These results allow us to speculate about fundamental tradeoffs: What are potential advantages and disadvantages to hierarchical rich-club structure? On the one hand, more distributed con-

nectivity may be advantageous in that it leads to more distributed collective modes, longer timescales, and therefore better averages over the noisy knowledge of individuals. On the other hand, the localized modes created by a rich club structure could be advantageous for modularized function and localized control. In this way, the rich club could be a way to bring only a subset of the system supercritical, with consequently reduced noise-reduction benefits of collectivity.

We expect this framework and intuition to be useful in systems in which the interaction structure remains fixed over the timescale of a single decision process, but may vary over longer adaptive timescales. Besides neural dynamics, such a framework may be useful for describing genetic regulatory networks producing cell fate decisions during development [47], social networks producing consensus about dominance hierarchies [48], and networks of influence underlying decisions by political bodies [49, 50]. In such systems, the computation of decisions happens on relatively fast timescales, while on longer adaptive timescales, there may be tuning of the network that could change the relevant parameters λ_c and p.

To guide our intuition, our analysis focused on the simplest symmetry-breaking bifurcation, where the initial state of each individual is the same ($\vec{s}_0 = \vec{0}$). It will be useful in future work to focus on more complicated transitions (as explored in [38]), where we expect that differing states and therefore saturations across individuals will modify the calculation, perhaps leading to a generalized form of the participation ratio that weights individuals by their contributions.

Acknowledgments

Appendix

Derivation of distance between stable fixed points

The normal form of a system undergoing a pitchfork bifurcation is

$$\frac{d\nu}{dt} = a\nu + b\frac{\nu^3}{6}. \tag{7}$$

In a one-dimensional system with state x and dynamics $dx/dt = F(x)$ that has a pitchfork bifurcation at $x = x_0$, the system is described by Eq. (7) near x_0, with $\nu = x - x_0$, $a = dF(x)/dx|_{x=x_0}$, and $b = d^3F(x)/dx^3|_{x=x_0}$. This is the Taylor series of $F(x)$ at $x = x_0$ up to third order, where the second-order term disappears due to the symmetry that is required for a pitchfork bifurcation: $F(x_0 + \delta) = -F(x_0 - \delta)$ near $\delta = 0$. The bifurcation happens when a changes sign. We focus here on the case that creates two stable fixed points (decision states), which coincides with $b < 0$.

Solving Eq. (7) for $d\nu/dt = 0$, we find one fixed point at $\nu^* = \nu_0$ that changes from stable when $a < 0$ to unstable when $a > 0$, and two stable fixed points when $a > 0$ at

$$\nu^* = \pm\sqrt{6a/|b|}. \tag{8}$$

For example, in a simple one-dimensional case where $F(x) = -x + \mu \tanh x$, we have $\nu = x$, $x_0 = 0$, $a = \mu - 1$, and $b = -2\mu$. Inserting into Eq. (8), we find, for small $\Delta\mu \equiv \mu - 1$, $\nu^* \approx \pm\sqrt{3\Delta\mu}$.

In the higher-dimensional context of Eq. (1), ν becomes the linear combination of state $\vec{s}$ along the dimension of the least-stable dimension $\hat{e}_c$: $\nu = \vec{s} \cdot \hat{e}_c$. Then, to produce the Taylor series corresponding to Eq. (7), we take the relevant directional derivatives of the right-hand side of Eq. (1). Calling the zero-noise, zero-input part of the dynamics $\vec{F}$ [that is, $F_i(\vec{s}) = -s_i + \mu \sum_j A_{ij} \tanh(s_j)$], we have

$$a = \hat{e}_c \cdot \frac{\partial \vec{F}(\vec{s})}{\partial \nu}\Big|_{\vec{s}=\vec{0}} = \hat{e}_c \cdot (\nabla F \cdot \hat{e}_c)|_{\vec{s}=\vec{0}} = \mu\, \hat{e}_c^T A \hat{e}_c - 1 = \mu\lambda_c - 1; \tag{9}$$

$$b = \hat{e}_c \cdot \frac{\partial^3 \vec{F}(\vec{s})}{\partial \nu^3}\Big|_{\vec{s}=\vec{0}} = \hat{e}_c \cdot (\nabla(\nabla(\nabla F \cdot \hat{e}_c) \cdot \hat{e}_c) \cdot \hat{e}_c)|_{\vec{s}=\vec{0}} = -2\mu\lambda \sum_i (\hat{e}_c)_i^4. \tag{10}$$

Inserting this into Eq. (8) produces

$$\nu^* = \pm\sqrt{3p\frac{\mu - \mu_c}{\mu}} = \pm\sqrt{3\bar{\mu}p} + O(\Delta\mu^{3/2}), \tag{11}$$

where $\mu_c = 1/\lambda_c$, $p = 1/\sum_i(\hat{e}_c)_i^4$, $\Delta\mu = \mu - \mu_c$, and $\bar{\mu} = \Delta\mu/\mu_c$.

We note that the above result assumes that the adjacency matrix A is symmetric. In the asymmetric case,

$$\nu^* \approx \sqrt{3\bar{\mu}\frac{\lambda_c}{(A^T \cdot \hat{e}_c) \cdot (\hat{e}_c)^3}}, \tag{12}$$

where $\hat{e}_c$ is the normalized eigenvector of A corresponding to λ_c.

Derivation of approximate decision timescale t_D

We define the decision timescale t_D as the time for $\nu = |\vec{s} \cdot \hat{s}^*|$ to reach halfway to the fixed point ν^*. To approximate t_D in the presence of noise, we patch together two types of behavior. First, for sufficiently small times t, we expect the average behavior along $\hat{e}_c$ to be dominated by noise [the ξ term dominates in Eq. (1)]. Noise dominates here because the system is still close to the fixed point at the origin, where, at the bifurcation, the first two terms cancel up to second order in ν. Neglecting all terms other than the noise term, the average behavior is given by $\langle\nu_1(t)\rangle = \sigma\sqrt{t/\tau}$. Then, after a crossing time t_{cross}, the first two terms dominate and noise becomes unimportant. Now neglecting the noise term, given an initial condition of $\nu_0 = \langle\nu_1(t_{\text{cross}})\rangle$, and considering for simplicity only the lowest-order approximation of F near the unstable fixed point, the state simply grows exponentially: $\langle\nu_2(t)\rangle = \nu_0 \exp(t - t_{\text{cross}})\bar{\mu}/\tau$.

We patch these two solutions together by defining t_{cross} as the time when their derivative matches:

$$d\langle\nu_1(t)\rangle/dt|_{t=t_{\text{cross}}} = d\langle\nu_2(t)\rangle/dt|_{t=t_{\text{cross}}}.$$

Solving this produces $t_{\text{cross}} = y\tau/\bar{\mu}$, where $y \approx 0.3517$ is the solution to $2\exp y = y^{-1}$. Finally, we solve for t_D, the time to reach $\nu^*/2$, as a function of the reduced distance from the transition $\bar{\mu}$:

$$t_D(\bar{\mu}) = \begin{cases} \frac{3p\bar{\mu}}{4\sigma^2}\tau & \bar{\mu} < \bar{\mu}_{\text{cross}}, \\ \frac{\tau}{2\bar{\mu}}\left(2y + \log\frac{3p\bar{\mu}^2}{4y\sigma^2}\right) & \bar{\mu} \geq \bar{\mu}_{\text{cross}}, \end{cases} \tag{13}$$

where $\bar{\mu}_{\text{cross}} = 2\sigma\sqrt{y/3p}$. This approximation of the decision timescale is plotted in Figure 4 as dashed

and solid lines (dashed for $\bar{\mu} < \bar{\mu}_{\mathrm{cross}}$ and solid for $\bar{\mu} > \bar{\mu}_{\mathrm{cross}}$). The function $t_D(\bar{\mu})$ has a maximum at $\bar{\mu}_{\mathrm{max}} = \bar{\mu}_{\mathrm{cross}} \exp(1 - y)$, producing the maximal decision timescale for a given transition as

$$t_D^{\mathrm{max}} = \frac{\tau z \sqrt{3p}}{2\sigma}, \tag{14}$$

where $z = e^{y-1}/\sqrt{y} \approx 0.882$.

Impact of noise on the critical point

In order to asses the general impact of noise on the critical coupling strength μ_c, we consider a mean-field approach (fully connected graph) in the absence of an external signal ($I = 0$). The general approach employed here is analogous to the one used in [51, 52], where a more detailed account can be found. The mean field stochastic differential equation corresponding to Eq. 1 reads:

$$\frac{ds_i}{dt} = -\frac{s}{\tau} + \frac{\tilde{\mu}}{\tau}\langle \tanh s \rangle + \xi \tag{15}$$

Here $\langle \tanh s \rangle$ represents the expectation value of the interaction term, and $\tilde{\mu} = N\mu$ is the mean field coupling strength scaled by the number of nodes N. Assuming $s \ll 1$, we use the Taylor expansion $\tanh x \approx x - x^3/3$ to rewrite the interaction of the individual node with the mean field in terms of the first and third moment of s:

$$\frac{ds_i}{dt} = -\frac{s}{\tau} + \frac{\tilde{\mu}}{\tau}\left(\langle s \rangle - \frac{1}{3}\langle s^3 \rangle\right) + \xi \tag{16}$$

From the above stochastic differential equation we can derive the following nonlinear Fokker-Planck equation for the probability density function (PDF) $p(s,t) = \langle \frac{1}{N}\sum_j \delta(s - s_j)\rangle$:

$$\tau\partial_t p(s,t) = -\partial_s\left\{\left[-s + \tilde{\mu}\left(\langle s \rangle - \frac{1}{3}\langle s^3 \rangle\right)\right]p(s,t)\right\} + \frac{\sigma^2}{2}\partial_s^2 p(s,t) \tag{17}$$

Here, the crucial simplifying assumption in the derivation is that the N-particle distribution function factorizes, i.e. that the correlations between nodes can be neglected (*mean-field ansatz*).

Inserting Eq. 17 into

$$\partial_t\langle s^n \rangle = \partial_t \int_{-\infty}^{\infty} s^n p(s,t)\mathrm{d}s = \int_{-\infty}^{\infty} s^n \partial_t p(s,t)\mathrm{d}s \tag{18}$$

produces a hierarchy of coupled evolution equations for the different moments $\langle s^n \rangle$ of the PDF.

We rewrite the state variable as $s = u + \delta s$, where u is the average state of the system and δs is the fluctuation around the mean, and assume that $\langle \delta s^k \rangle = 0$ for all odd k ($k = 1, 3, 5, \ldots$). This allows us to express the first three moments of $p(s,t)$ as:

$$\langle s \rangle = u \tag{19}$$
$$\langle s^2 \rangle = u^2 + \langle \delta s^2 \rangle \tag{20}$$
$$\langle s^3 \rangle = u^3 + 3u\langle \delta s^2 \rangle \tag{21}$$

In the following, we will use the notation $T = \langle \delta s^2 \rangle$ for the variance of the fluctuations. It can be viewed as an effective "temperature" quantifying the intensity of the fluctuations around the mean.

Eventually combining equations 17, 18 and 19 we arrive at the following evolution equations for the mean u and the temperature T:

$$\partial_t u = u \frac{1}{\tau} \left[\tilde{\mu} - 1 - \frac{\tilde{\mu}}{3} \left(u^2 + 3T \right) \right] \tag{22}$$

$$\partial_t T = \frac{1}{\tau} \left(\sigma^2 - 2T \right) \tag{23}$$

The corresponding stationary solutions can be easily obtained by solving the above equations for $\partial_t u = \partial_t T = 0$. The stationary temperature T^* is

$$T^* = \frac{\sigma^2}{2} \tag{24}$$

The cubic equation for the mean yields three stationary solutions u^*, which correspond directly to the fixed points ν^* discussed in the context of the general pitch-fork bifurcation above:

$$u_1^* = 0 \tag{25}$$

$$u_{2,3}^* = \pm \sqrt{\frac{3}{\tilde{\mu}} (\tilde{\mu} - 1) - \frac{3\sigma^2}{2}} \tag{26}$$

Here, the u_1^* corresponds to the disordered solution below a critical coupling strength. If the coupling strength becomes too large, then this disordered solution becomes unstable. In the absence of an external signal (bias), we observe a spontaneous symmetry breaking, where $u_{2,3}^*$ correspond to the two possible solutions, identical with the two different branches of the pitchfork. These two stationary solutions exist only if the argument in the square root is positive (as $u^* \in \mathbb{R}$).

For vanishing noise, $\sigma^2 = 0$, the critical mean-field coupling strength is $\tilde{\mu}_c = 1$, which is consistent with our previous results if we consider a fully connected graph. For small noise $\sigma \ll 1$ the critical point is modified according to:

$$\tilde{\mu}_c = \frac{1}{1 - \frac{\sigma^2}{2}} \approx 1 + \frac{\sigma^2}{2} \tag{27}$$

Thus, introducing noise leads effectively only to a shift of the critical coupling strength to larger values, without any qualitative change regarding general result obtained for the zero noise case. Furthermore, the shift is small for the regime we test in this study: with $\sigma = 0.05$ we expect corrections to μ_c on the order of 10^{-3}.

References

[1] Jolle W Jolles, Neeltje J Boogert, Vivek H Sridhar, Iain D Couzin, and Andrea Manica. Consistent individual differences drive collective behavior and group functioning of schooling fish. *Current Biology*, 27(18):2862–2868, 2017.

[2] David Bierbach, Tim Landgraf, Pawel Romanczuk, Juliane Lukas, Hai Nguyen, Max Wolf, and Jens

Krause. Using a robotic fish to investigate individual differences in social responsiveness in the guppy. *Royal Society Open Science*, 5, 2018.

[3] Iain D Couzin, Christos C Ioannou, Güven Demirel, Thilo Gross, Colin J Torney, Andrew Hartnett, Larissa Conradt, Simon A Levin, and Naomi E Leonard. Uninformed individuals promote democratic consensus in animal groups. *science*, 334(6062):1578–1580, 2011.

[4] Itai Pinkoviezky, Iain D Couzin, and Nir S Gov. Collective conflict resolution in groups on the move. *Physical Review E*, 97(3):032304, 2018.

[5] Bryan C Daniels, David C Krakauer, and Jessica C Flack. Sparse code of conflict in a primate society. *Proceedings of the National Academy of Sciences*, 109(35):14259–14264, 2012.

[6] Bryan C Daniels, David C Krakauer, and Jessica C Flack. Control of finite critical behaviour in a small-scale social system. *Nature communications*, 8:14301, 2017.

[7] Logan Harriger, Martijn P. van den Heuvel, and Olaf Sporns. Rich Club Organization of Macaque Cerebral Cortex and Its Role in Network Communication. *PLoS ONE*, 7(9), 2012.

[8] S. Nigam, M. Shimono, S. Ito, F.-C. Yeh, N. Timme, M. Myroshnychenko, C. C. Lapish, Z. Tosi, P. Hottowy, W. C. Smith, S. C. Masmanidis, A. M. Litke, O. Sporns, and J. M. Beggs. Rich-Club Organization in Effective Connectivity among Cortical Neurons. *Journal of Neuroscience*, 36(3):670–684, 2016.

[9] Larissa Conradt and Timothy J Roper. Consensus decision making in animals. *Trends in ecology & evolution*, 20(8):449–456, 2005.

[10] John RG Dyer, Anders Johansson, Dirk Helbing, Iain D Couzin, and Jens Krause. Leadership, consensus decision making and collective behaviour in humans. *Philosophical Transactions of the Royal Society B: Biological Sciences*, 364(1518):781–789, 2008.

[11] Max Wolf, Ralf HJM Kurvers, Ashley JW Ward, Stefan Krause, and Jens Krause. Accurate decisions in an uncertain world: collective cognition increases true positives while decreasing false positives. *Proceedings of the Royal Society B: Biological Sciences*, 280(1756):20122777, 2013.

[12] Vittoria Colizza, Alessandro Flammini, M. Angeles Serrano, and Alessandro Vespignani. Detecting rich-club ordering in complex networks. *Nature Physics*, 2(February):110, 2006.

[13] Mordechai Z Juni and Miguel P Eckstein. Flexible human collective wisdom. *Journal of experimental psychology: human perception and performance*, 41(6):1588, 2015.

[14] Michael Kearns, Stephen Judd, Jinsong Tan, and Jennifer Wortman. Behavioral experiments on biased voting on networks. *Proc Natl Acad Sci U S A*, 106(5):1347–1352, 2009.

[15] Stephen Judd, Michael Kearns, and Yevgeniy Vorobeychik. Behavioral dynamics and influence in networked coloring and consensus. *Proceedings of the National Academy of Sciences*, 107(34):14978–14982, 2010.

[16] Sara Brin Rosenthal, Colin R Twomey, Andrew T Hartnett, Hai Shan Wu, and Iain D Couzin. Revealing the hidden networks of interaction in mobile animal groups allows prediction of complex behavioral contagion. *Proceedings of the National Academy of Sciences*, 112(15):4690–4695, 2015.

[17] Joaquin Navajas, Tamara Niella, Gerry Garbulsky, Bahador Bahrami, and Mariano Sigman. Aggregated knowledge from a small number of debates outperforms the wisdom of large crowds. *Nature Human Behaviour*, 2(2):126, 2018.

[18] Reza Olfati-Saber and Richard M Murray. Consensus problems in networks of agents with switching topology and time-delays. *IEEE Transactions on automatic control*, 49(9):1520–1533, 2004.

[19] Alex Arenas, Albert Díaz-Guilera, Jurgen Kurths, Yamir Moreno, and Changsong Zhou. Synchronization in complex networks. *Physics reports*, 469(3):93–153, 2008.

[20] Thilo Gross and Bernd Blasius. Adaptive coevolutionary networks: a review. *Journal of the Royal Society Interface*, 5(20):259–271, 2007.

[21] Balazs Kozma and Alain Barrat. Consensus formation on adaptive networks. *Physical Review E*, 77(1):016102, 2008.

[22] Thierry Mora and William Bialek. Are biological systems poised at criticality? *Journal of Statistical Physics*, 144(2):268–302, 2011.

[23] Giuseppe Carbone and Ilaria Giannoccaro. Model of human collective decision-making in complex environments. *The European Physical Journal B*, 88(12):339, 2015.

[24] Paolo Moretti and Miguel A. Muñoz. Griffiths phases and the stretching of criticality in brain networks. *Nature Communications*, 4:2521, 2013.

[25] Ravi Kumar, Jasmine Novak, and Andrew Tomkins. Structure and evolution of online social networks. In *Link mining: models, algorithms, and applications*, pages 337–357. Springer, 2010.

[26] Michelle Girvan and Mark EJ Newman. Community structure in social and biological networks. *Proceedings of the national academy of sciences*, 99(12):7821–7826, 2002.

[27] S Boccaletti, M Ivanchenko, V Latora, A Pluchino, and A Rapisarda. Detecting complex network modularity by dynamical clustering. *Physical Review E*, 75(4):045102, 2007.

[28] M. P. van den Heuvel and O. Sporns. Rich-Club Organization of the Human Connectome. *Journal of Neuroscience*, 31(44):15775–15786, 2011.

[29] Danielle S. Bassett, Nicholas F. Wymbs, M. Puck Rombach, Mason A. Porter, Peter J. Mucha, and Scott T. Grafton. Task-Based Core-Periphery Organization of Human Brain Dynamics. *PLoS Computational Biology*, 9(9):1–16, 2013.

[30] Leonardo L. Gollo, Andrew Zalesky, R. Matthew Hutchison, Martijn van den Heuvel, and Michael Breakspear. Dwelling quietly in the rich club: Brain network determinants of slow cortical fluctuations. *Philosophical Transactions of the Royal Society B: Biological Sciences*, 370(1668), 2015.

[31] Yannick Leo, Eric Fleury, J. Ignacio Alvarez-Hamelin, Carlos Sarraute, and Marton Karsai. Socioeconomic correlations and stratification in social-communication networks. *Journal of the Royal Society Interface*, 13(125), 2016.

[32] Mario Senden, Gustavo Deco, Marcel A de Reus, Rainer Goebel, and Martijn P van den Heuvel. Rich club organization supports a diverse set of functional network configurations. *Neuroimage*, 96:174–182, 2014.

[33] Vaibhav Srivastava and Naomi Ehrich Leonard. Collective decision-making in ideal networks: The speed-accuracy tradeoff. *IEEE Transactions on Control of Network Systems*, 1(1):121–132, 2014.

[34] Xiao-Jing Wang. Probabilistic decision making by slow reverberation in cortical circuits. *Neuron*, 36(5):955–968, 2002.

[35] Bryan C. Daniels, Jessica C. Flack, and David C. Krakauer. Dual Coding Theory Explains Biphasic Collective Computation in Neural Decision-Making. *Frontiers in Neuroscience*, 11(June):1–16, 2017.

[36] Lars Chittka, Peter Skorupski, and Nigel E. Raine. Speed-accuracy tradeoffs in animal decision making. *Trends in Ecology and Evolution*, 24(7):400–407, 2009.

[37] James a R Marshall, Rafal Bogacz, Anna Dornhaus, Robert Planqué, Tim Kovacs, and Nigel R Franks. On optimal decision-making in brains and social insect colonies. *Journal of the Royal Society, Interface / the Royal Society*, 6(40):1065–74, nov 2009.

[38] Emerson Arehart, Tangxin Jin, and Bryan C. Daniels. Locating Decision-Making Circuits in a Heterogeneous Neural Network. *Frontiers in Applied Mathematics and Statistics*, 4(May):11, 2018.

[39] Nigel R. Franks, Anna Dornhaus, Jon P. Fitzsimmons, and Martin Stevens. Speed versus accuracy in collective decision making. *Proceedings of the Royal Society B: Biological Sciences*, 270(1532):2457–2463, 2003.

[40] Mark Newman. *Networks: An Introduction*. Oxford University Press, 2010.

[41] Vasiliki Plerou, Parameswaran Gopikrishnan, Bernd Rosenow, Luís A.Nunes Amaral, Thomas Guhr, and H Eugene Stanley. Random matrix approach to cross correlations in financial data. *Physical Review E*, 65(6):066126, 2002.

[42] F L Metz, I Neri, and D. Bollé. Localization transition in symmetric random matrices. *Physical Review E*, 82(3):031135, 2010.

[43] Surya Ganguli, James W. Bisley, Jamie D. Roitman, Michael N. Shadlen, Michael E. Goldberg, and Kenneth D. Miller. One-Dimensional Dynamics of Attention and Decision Making in LIP. *Neuron*, 58:15–25, 2008.

[44] Francesca Mastrogiuseppe and Srdjan Ostojic. Linking Connectivity, Dynamics, and Computations in Low-Rank Recurrent Neural Networks. *Neuron*, 99:609–623, 2018.

[45] A. V. Goltsev, S. N. Dorogovtsev, J. G. Oliveira, and J. F.F. Mendes. Localization and spreading of diseases in complex networks. *Physical Review Letters*, 109(12):1–5, 2012.

[46] Yan V. Fyodorov and Alexander D. Mirlin. Analytical Derivation of the Scaling Law for the Inverse Participation Ratio in Quasi-One-Dimensional Disordered Systems. *Physical Review Letters*, 69:1093, 1992.

[47] Mitra Mojtahedi, Alexander Skupin, Joseph Zhou, Ivan G Castaño, Rebecca Y Y Leong-Quong, Hannah Chang, Kalliopi Trachana, Alessandro Giuliani, and Sui Huang. Cell Fate Decision as High-Dimensional Critical State Transition. *PLoS Biology*, 14(12):e2000640, 2016.

[48] Eleanor R Brush, David C Krakauer, and Jessica C Flack. A family of algorithms for computing consensus about node state from network data. *PLoS computational biology*, 9(7):e1003109, jan 2013.

[49] Edward D. Lee, Chase P. Broedersz, and William Bialek. Statistical Mechanics of the US Supreme Court. *Journal of Statistical Physics*, 160(2):275–301, 2015.

[50] Alexander T. J. Barron, Jenny Huang, Rebecca L. Spang, and Simon DeDeo. Individuals, Institutions, and Innovation in the Debates of the French Revolution. *Proceedings of the National Academy of Sciences of the United States of America*, 115(18):4607–4612, 2018.

[51] Pawel Romanczuk and Udo Erdmann. Collective motion of active brownian particles in one dimension. *The European Physical Journal Special Topics*, 187(1):127–134, 2010.

[52] Robert Grossmann, Lutz Schimansky-Geier, and Pawel Romanczuk. Active brownian particles with velocity-alignment and active fluctuations. *New Journal of Physics*, 14(7):073033, 2012.